Check for
updates

Permeability and Mechanical Properties of Additively Manufactured Porous Maraging 300 Steel

Shen Huei Wynton Lee[1] · Hui Leng Choo[1] · Sui Him Mok[2] · Xin Yi Cheng[3] ·
Yupiter Harangan Prasada Manurung[4]

Abstract

Porous metallic materials are materials that have closed cell or open cell pores within their microstructure and have unique properties such as permeability and high stiffness-to-weight ratio depending on the type of the pore. Open cell pores in porous metallic materials allow minuscule particles such as air to pass through, giving it its permeability property. Permeability in porous metallic materials can further serve as air vents in injection moulds allowing the process to have a better surface finish and also dispel heat from the system better. Additive manufacturing can manufacture these materials to save time and cost and provides more intricate designs compared to traditional manufacturing. This study aims to manufacture maraging 300 steel with tailored porosity by controlling the processing parameters in the selective laser melting (SLM) process. The effect of each parameter on relative density was determined using an L9 orthogonal array through Taguchi's Design of Experiments. It was found that hatch spacing had the largest effect, followed by laser power, layer thickness, and scanning speed. Regression modelling found that the equation can provide a good prediction of the relative density. When the processing parameters were related to energy density function, regression equation utilising energy density has a better performance, but its use is restricted to the range of energy density reported. The materials became permeable when the relative density is less than 95%. Permeability increases linearly with a sharp increase at a relative density below 80% due to the high volume of open pores. In terms of mechanical properties, both compression modulus and yield strength decrease with decreasing relative density. The method shown here can be applied to produce, within the same part, a combination of porous and non-porous sections in the same manufacturing process.

Keywords Porous metal · Permeability · Selective laser melting · Energy density · Processing parameter · Mechanical properties

✉ Hui Leng Choo
HuiLeng.Choo@taylors.edu.my

Extended author information available on the last page of the article

Introduction

Porous metallic materials, also known as metal foams, are materials that contain air pockets or pores within the structure. The presence of pores in these materials make the material lighter and can provide a unique combination of physical and mechanical properties as compared to the full density materials depending on the type of pores [1]. Porous metallic materials can be used for heat exchangers, mechanical vibration damping, sound absorption, filters, thermal energy storage systems and medical implants [2–4]. Traditionally, metal foams are manufactured in standard shapes and sizes which requires further post-processing to obtain the desired shape [5]. This leads to a lot of material and time wasted to manufacture these porous metallic materials.

With the emergence of additive manufacturing (AM) in recent decades, components can be manufactured to their desired shape with minimal post-processing. The different types of AM methods are Material Extrusion, Direct Energy Deposition (DED), Powder Bed Fusion, Photopolymerization, Binder Jetting, Material Jetting and Sheet Lamination [6]. Different AM methods are tailored for different types of materials; DED and Powder Bed Fusion can manufacture metal components and selective laser melting (SLM) is a form of Powder Bed Fusion. Porous metallic materials can be used for many applications such as injection moulding technology and bio-implants. Internal cooling paths in injection moulds could be designed and fabricated through AM which would be almost impossible in traditional manufacturing methods [7]. Porous microstructures in bio-implants would assist in cell culture and fabricating of the implants would be a lot faster through AM by scanning the bone structure of medical patients and converting it into a 3D CAD file [8].

Porous metallic materials can be produced in a one-stage process where the component can be designed to have porous structures by utilizing unit cells. Unit cells are tiny structures that have a specific shape and do not occupy the full volume of its bulk dimension. When unit cells are combined, they form lattice structures with voids that fill up the whole component in the CAD file, making it a porous component [9, 10]. However, designing AM components with unit cells can be time-consuming and may require high computing power. Another method that can be used to manufacture porous metallic materials is by the energy density modification method. Energy density is the amount of energy applied per unit volume on the metal powder. When the energy density is lower, some materials on the bed would not be melted and there is no fusion between particles forming a hollow region in the microstructure of the component. The benefits of producing porous metallic materials through SLM would eliminate material waste through post processing on metal components with complex shapes. The pores formed in the microstructure of the SLM component would enhance its overall heat exchanging properties throughout the whole component and also allow pores to be formed in areas that are difficult to manufacture cavities through traditional manufacturing.

Melting of the material in the laser melting process can be grouped into four categories: I) no melting, II) partial melting, III) melting with the balling phenomenon and IV) complete melting [11]. When the energy density of the process is lower, the balling effect occurs, and pores are formed in the specimen. Energy density, E_D (J/mm^3), can be related to four different processing parameters in the SLM process as shown in Eq. 1 [12]:

$$E_D = \frac{P}{v \cdot h \cdot t} \tag{1}$$

where P is the laser power (W), v is scanning speed (mm/s), h is the hatch spacing (mm) and t is the layer thickness (mm).

Many studies on the effects of processing parameters largely focused on obtaining full density parts [12–18]. Studies have shown that porous metallic materials can be manufactured by varying the processing parameters [19–27]. However, the studies usually focused selectively on a few processing parameters and there is currently no publication on producing porous maraging steel. Scanning speed was found to be one of the largest contributors towards the formation of pores when fabricating stainless steel 316 L (SS316L) alongside laser power as another major contributor [28]. Hatch spacing was found to have the least effect on the porosity of the SS316L metal powder [14].

Open pores formed in porous metallic materials allow small particles or fluids to pass through depending on the size of the pores. When objects are able to pass through the material, the material is produced with a certain degree of permeability. Permeability in porous metallic materials is believed to enhance the material by allowing it to serve as an air vent which will contribute greatly in injection mould inserts. When plastic is being injected into the mould in the injection mould process, existing air in the mould cavity is required to purge from the mould. However, when the two mould inserts are clamped tight, it makes it extremely difficult for the air to escape. Hence, permeability in injection moulds will assist the air to escape from the mould easier. The permeability of the injection moulds, however, have to be greatly controlled to only allow air to pass through and not the moulded plastic. Fabricating porous injection moulds with permeability and through the SLM process, allows manufacturers to have moulds that serve as air vents and also able to fabricate the moulds in a one-step process.

Currently, there is no method to fabricate tailored porosity maraging steel components using energy density modification method based on past literature review. Therefore, this research aims to study the effects of each processing parameter on the porosity and to develop a method to fabricate tailored porosity components by using Taguchi Design of Experiments. The fabrication of porous metallic materials with desired porosity through AM has the potential for application in many industries especially for those that need components with specific porosity to reduce material usage, manufacturing cost, and weight. This study focused on the fabrication of porous metallic materials by SLM process through the energy density modification method instead of the unit cell structure method. The latter which integrates unit cells within the microstructure of the component through topology optimization heavily relies on computing power and also time used to design and implement the unit cells in the microstructure which is out of the scope of this study.

Material and Methods

Material

The metal powder used was maraging 300 steel (Tool Steel 1.2709) supplied by SLM Solutions. Tool Steel 1.2709 was chosen as it is used for manufacturing moulds,

Table 1 Chemical composition of Tool Steel 1.2709 (% mass fraction)

Element	Fe	Ni	Co	Mo	Ti	Al	Mn	Si	P	S	C
% mass	Bal.	18–19	8.5–9.5	4.7–5.2	0.5–0.8	0.05–0.15	0.1	0.1	0.01	0.01	0.03

engineering parts, automotive and aerospace applications. The chemical composition of the material is shown in Table 1.

Design of Experiments

To understand the effects of the processing parameters in the SLM process on the relative density of the AM parts, Taguchi's Design of Experiments (DOE) method was used. An L_9 orthogonal array which is suitable for the study of four three-level factors was used. The investigated processing parameters, along with the range of values are shown in Table 2. The four parameters were chosen as they can be used to calculate energy density based on Eq. 1 and are easy to control within the machine manufacturer's software. The values were chosen to ensure that the resulting energy density will always be less than when the standard parameters are used to promote porosity.

The populated L_9 orthogonal array is shown in Table 3. The values of E_D were calculated using Eq. 1. The E_D using standard parameters is 69.4 J/mm^3 and Run 1–9 have values below that.

In Taguchi's approach of DOE, the signal-to-noise (S/N) ratio is used to analyse the data and to find the optimum factor values for a certain desired response. S/N ratio analysis is used in Taguchi's method because S/N ratio represents the mean and scatter of the result in the experiment. There are three main types of analysis for S/N ratio used in Taguchi's method: 1) smaller-the-better; 2) nominal-the-best; 3) larger-the-better. Since this research is focused on achieving low relative density, the smaller-the-better type of S/N ratio analysis was used. The smaller-the-better S/N ratio can be calculated from Eq. 2:

$$S/N = -10\log\left[\frac{1}{n}\sum_{i=1}^{n}\left(y_i^2\right)\right] \tag{2}$$

where n is the number of specimens for each run and y_i is the individual response of each

Table 2 Processing Parameters and their levels

Processing Parameters	Standard Values	Levels		
		1	2	3
Laser Power, P (W)	200	150	175	200
Scanning Speed, v (mm/s)	800	800	900	1000
Layer Thickness, t (mm)	0.03	0.03	0.04	0.05
Hatch Spacing, h (mm)	0.12	0.12	0.24	0.36

Table 3 Taguchi L$_9$ orthogonal array with four three-levels factors, including the calculated E_D

Run	Laser Power, P (W)	Scanning Speed, v (mm/s)	Layer Thickness, t (mm)	Hatch Spacing, h (mm)	Energy Density, E_D (J/mm^3)
1	150	800	0.03	0.12	52.1
2	150	900	0.04	0.24	17.4
3	150	1000	0.05	0.36	8.3
4	175	800	0.04	0.36	15.2
5	175	900	0.05	0.12	32.4
6	175	1000	0.03	0.24	24.3
7	200	800	0.05	0.24	20.8
8	200	900	0.03	0.36	20.6
9	200	1000	0.04	0.12	41.7
Standard Parameter	200	800	0.03	0.12	69.4

specimen. In this case, the response would be the relative density.

Analysis of Variance (ANOVA) was also carried out to examine the contribution and importance of each processing parameter on the relative density of the specimens. Finally, a regression model was generated to estimate the relative density based on the four processing parameters. Statistical analysis in this research was carried out using Minitab 19.

Manufacturing Process

The fabrication of the specimens was carried out using an SLM280 machine from SLM Solutions. It has a maximum build volume of $280 \times 280 \times 365$ mm^3 and equipped with two 700 W lasers with an 80 μm spot diameter. The manufacturing was carried out in an argon atmosphere. Cylindrical specimens with dimensions of 15 mm in diameter and 25 mm height were produced for relative density and compression properties measurement. For permeability measurement, the specimens were 15 mm in diameter with a full density skin of 5 mm around it and 3 mm in height. Three specimens were produced for every run to increase the accuracy of the measurement. The order of the run was randomized to reduce error. Specimens were removed from the build plate using a wire cutter and ground to size. All specimens were used as is without heat treatment.

Relative Density Measurement

Relative density was measured using the Archimedes method. The specimens were dried in a convection oven at 60 °C for 2 h to remove all the moisture retained in the microstructure. The dry mass of the specimens, m_{Dry} (g), were weighed and the exterior volume of the specimens, $V_{Exterior}$ (cm^3), were measured. The bulk density was calculated using Eq. 3.

$$\rho_{Bulk} = \frac{m_{Dry}}{V_{Exterior}}$$
(3)

The relative density of each specimen was then calculated using Eq. 4 by comparing the bulk density of the specimen to the density of Tool Steel 1.2709 which is 8 g/cm^3.

$$Relative\ Density, RD\ (\%) = \frac{\rho_{Bulk}}{\rho_{Tool\ Steel}} \times 100 \qquad (4)$$

Scanning Electron Microscope

Scanning Electron Microscope (SEM) images of the SLM specimens were taken using an SEC Desktop Mini-SEM SNE-3000 M at 100× magnification, 20 kV accelerated voltage, and under high vacuum condition. The formation of the struts and the pores in the structure of the fabricated specimens were observed from these images.

Permeability Test

The permeability of the porous metallic specimens was measured with a specially designed and constructed apparatus according to Furumoto et al [24]. The apparatus consists of two pressure gauges and regulators to measure and control the inlet and outlet pressure and a specimen holder, as shown in Fig. 1.

Compressed air with a pressure of 3 bar was used at the inlet. A digital anemometer was used to measure the volumetric flow rate of the compressed air at the outlet. The permeability, φ (m^2), of each specimen was calculated using Eq. 5 [24]:

$$\varphi = \dot{V}\mu\frac{t}{A}\frac{1}{P_1 - P_2} \qquad (5)$$

where $\dot{V}$ is the volumetric flow rate of the fluid (m^3/s), μ is the dynamic viscosity of the fluid (Pa·s), t is the thickness of the specimen (m), A is the cross-sectional area of the fluid passing through the specimen (m^2), and P_1 and P_2 are the inlet and the outlet pressure, respectively (Pa).
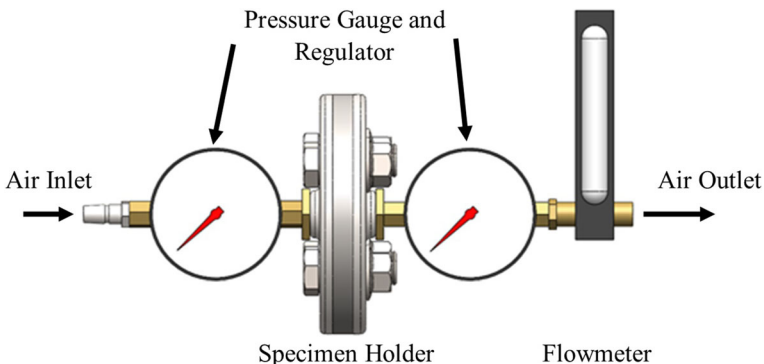

Fig. 1 Apparatus used to measure the permeability of the porous specimens

Compression Properties

Compression tests were carried out using a GO-TECH Testing Machine equipped with a 500 kN load cell following the ASTM E9 standard. Cylindrical specimens were used and tested at a strain rate of 0.005 m/m-min. Compression elastic modulus and compression yield strength (0.2% offset) were obtained according to the standard.

Results and Discussion

Fabricated Specimens

All the specimens were successfully fabricated, and the specimens formed using the highest and the lowest energy density are shown in Fig. 2. At the lowest energy density, pores can be seen on the specimens without a microscope (Fig. 2b and d) whereas there were no visible pores for the highest energy density specimens (Fig. 2a and c). The coin samples also show that both porous and non-porous sections can be built into the same part in the same manufacturing process.

Effects of Energy Density on Relative Density

The mean and standard deviation of the relative density of the specimens in each run is tabulated in Table 4. Overall, the standard deviation is less than 1% of the mean, demonstrating that the SLM process can produce porous specimens with high repeatability. When standard parameter values were used, the maximum relative density is $97.2 \pm 1.0\%$ whereas the lowest relative density obtained was 41%.
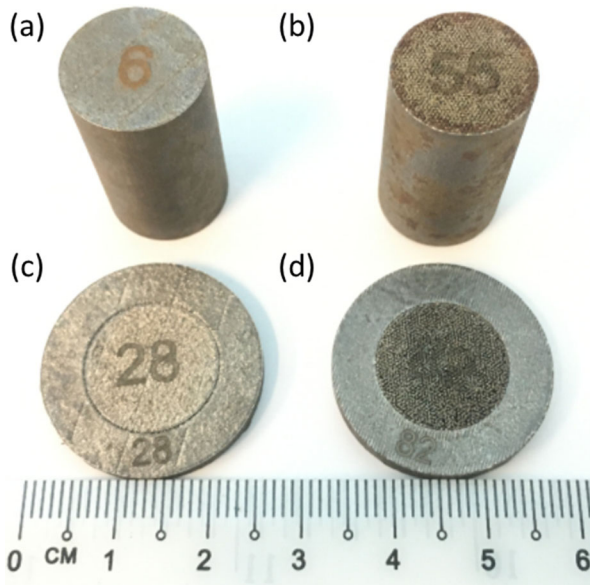

Fig. 2 Fabricated cylindrical specimens **a** Run 1 (52.1 J/mm^3) and **b** Run 3 (8.3 J/mm^3) and coin specimens **c** Run 1 (52.1 J/mm^3) and **d** Run 3 (8.3 J/mm^3)

Figure 3 shows the variation in relative density with energy density. As expected, the relative density increases with increasing energy density. This is because, at lower energy density, more materials are unmelted, forming hollow region. A similar trend was observed by other researchers for materials such as SS316L [14], alloy steel with copper phosphorous alloy and nickel [24], and titanium alloy [23]. For maraging steel, at energy density above 40 J/mm^3, relative density becomes asymptotic and is very close to the relative density achieved when using standard parameter values. The results show that a minimum relative density of 41% can be achieved, which is lower than that reported by other researchers for titanium alloys [20, 23]. Further reducing the relative density is expected to further deteriorate the surface finish.

Figure 4 shows the SEM images of the specimens at 100× magnification. When fabricated at the standard parameters, the specimen, shown in Fig. 4l, shows a good surface with no visible pores. Specimens fabricated at and below energy densities of 17.4 J/mm^3 produce pores as shown by the voids between the struts formed. In addition, the lower energy density in the SLM process leads to incomplete melting and the majority of the struts were not fully connected as shown in Fig. 4a–c, especially for the lowest energy density of 8.3 J/mm^3. At energy densities between 20 and 32 J/mm^3, the spacing between each struct is still present due to the large hatch spacing, the struts are however mostly connected, thus increasing their densities. This can be seen in Fig. 4d–f. At energy densities above 40 J/mm^3, there are no gaps between the struts as the lowest hatch spacing (0.12 mm) was used, which can be observed in Fig. 4g–i. However, some pores are still present between the struts in Fig. 4g and h, which are magnified to 500× and displayed in Fig. 4j and k. At above 50 J/mm^3, there are no visible pores present. Nevertheless, the struts are not as uniform as that formed when standard parameters were used.

Using the data from Table 4, a regression line to estimate the relative density based on energy density is shown in Eq. 6. A cubic equation was found to be a good fit with R^2 of 0.9951. This equation is only valid within the experimental range of energy density, which is 8–52 J/mm^3.

Table 4 Mean relative density and standard deviation at each run

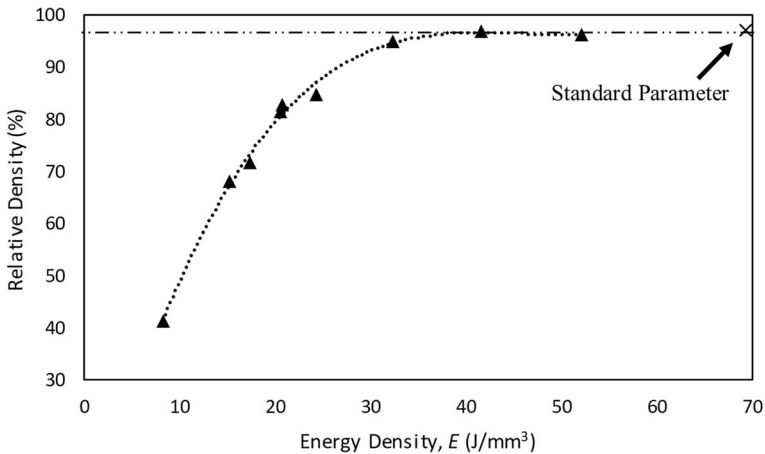| Run	Energy Density, E (J/mm^3)	Relative Density, RD (%)	
		Mean	Std. Dev.
1	52.1	96.3	0.3
2	17.4	71.7	0.7
3	8.3	41.3	0.2
4	15.2	68.3	0.7
5	32.4	95.1	0.3
6	24.3	84.8	0.4
7	20.8	82.7	0.9
8	20.6	81.5	0.4
9	41.7	96.8	0.2
Standard Parameter	69.4	97.2	1.0

Fig. 3 Graph of relative density against energy density. The dotted line is shown to illustrate the asymptotic behaviour only

$$RD_{ED} = 0.0011E^3 - 0.1493E^2 + 6.7768E - 5.0732 \qquad (6)$$

Effects of Processing Parameters on Relative Density

Table 5 shows the mean S/N ratio of each level, delta and the ranking of the parameters obtained using the smaller-the-better setting. The delta value is the difference between the largest and the smallest value between the three levels for each parameter. The larger the delta value, the higher the ranking of the parameter. Based on the results, hatch spacing has the most effect on the relative density followed by laser power, layer thickness, and scanning speed. The effects of hatch spacing can be observed in Fig. 4, where the lowest hatch spacing (0.12 mm) gave the highest density of struts within the same area. Previous research has also shown that larger hatch spacing gave rise to higher porosity [23, 26].

Figure 5 shows the effects plots of the four processing parameters towards the mean of the S/N ratios for relative density. Since the research focuses on high porosity and low relative density, the setting was to smaller-the-better. To achieve a lower relative density, laser power should be reduced whereas scanning speed, layer thickness, and hatch spacing should be increased. This confirms the relationship in Eq. 1 and shows that a decrease in energy density will result in decreasing relative density.

Anova Analysis

Results obtained from ANOVA are shown in Table 6. A confidence interval of 95% was used, resulting in F-critical value, $F_{0.05,2,18}$ of 3.55. Since all the F-values are above this, all the processing parameters influence the relative density, with hatch spacing having the biggest contribution, followed by laser power, layer thickness, and scanning speed. The results also confirmed the ranking provided by the Taguchi DOE. As all the P-values are below 0.05, this indicates that all parameters are significant and influence the relative density.
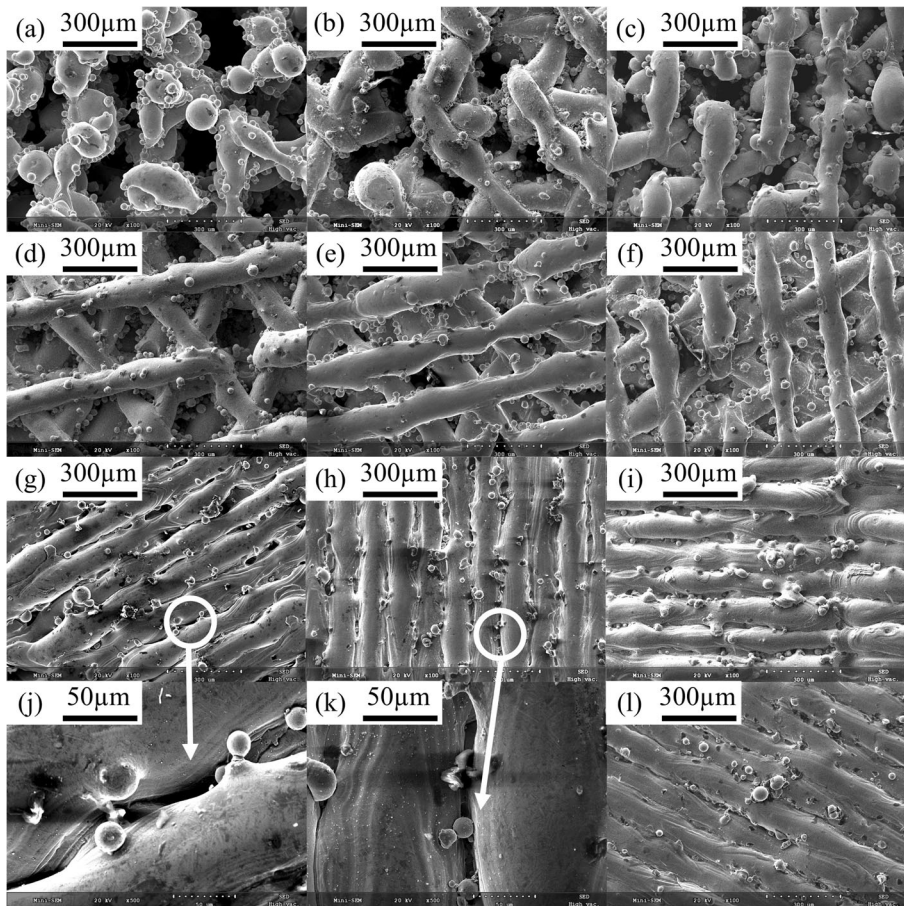
Fig. 4 SEM images of SLM specimens arranged at increasing energy density: **a** 8.3 J/mm³, **b** 15.2 J/mm³, **c** 17.4 J/mm³, **d** 20.6 J/mm³, **e** 20.8 J/mm³, **f** 24.3 J/mm³, **g**, **j** 32.4 J/mm³, **h**, **k** 41.7 J/mm³, **i** 52.1 J/mm³, and **l** 69.4 J/mm³

Regression Modelling

Regression modelling was carried out using Minitab 19 to produce a regression equation of relative density with respect to the four processing parameters as shown in Eq. 7. The R^2 value of the regression equation obtained is 96.79% which is satisfactory as a good fit equation.

Table 5 Response table of mean S/N ratios (smaller-the-better)

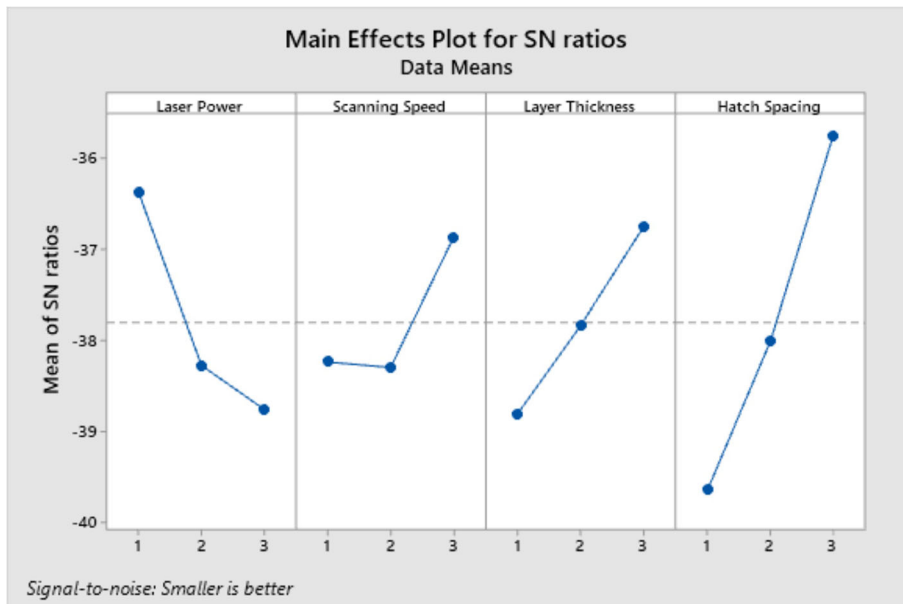| Level	Laser Power, P	Scanning Speed, v	Layer Thickness, t	Hatch Spacing, h
1	−36.37	−38.24	−38.82	−39.65
2	−38.28	−38.30	−37.84	−38.01
3	−38.76	−36.87	−36.74	−35.74
Delta	2.40	1.43	2.08	3.91
Rank	2	4	3	1

Fig. 5 Main effect plots for S/N ratios (smaller-the-better) of relative density in terms of laser power, scanning speed, layer thickness, and hatch spacing

$$RD_{DOE} = 117.5 + 0.3447P - 0.0407v - 724t - 134.9h \tag{7}$$

Verification Tests

To compare the performance of Eqs. 6 and 7 in estimating the relative density, additional specimens were fabricated according to the parameters in Table 7. The layer thickness was fixed to 0.03 mm and the laser power to 150 W. The other parameters were chosen randomly to ensure the energy density is between 10 and 20 J/mm^3. The experimental and estimated results are shown in Table 7. Both equations can predict the relative density reasonably well, with a maximum error of around 12%. However, Eq. 6 using E_D outperformed Eq. 7, showing that energy density is better at estimating the relative density.

Table 6 ANOVA results

Parameters	DF	Adj SS	Adj MS	F-Value	P Value
Laser Power	2	1452.14	726.07	2787.46	0.000
Scanning Speed	2	414.34	207.17	795.34	0.000
Layer Thickness	2	953.92	476.96	1831.09	0.000
Hatch Spacing	2	4715.57	2357.79	9051.75	0.000
Error	18	4.69	0.26		
Total	26	7540.66			

Table 7 Processing parameters for verification tests

Processing Parameters	Specimens		
	1	2	3
Layer Thickness, t (mm)	0.03	0.03	0.03
Laser Power, P (W)	150	150	150
Speed, v (mm/s)	1200	700	1000
Hatch Spacing, h (mm)	0.36	0.42	0.37
Energy Density, E_D (J/mm^3)	11.6	17.0	13.5
RD_{EXP} (%)	51.9	70.7	61.6
RD_{DOE} (%) – Eq. 7	50.1	62.3	56.9
Error (%)	3.6	11.8	7.7
RD_{ED} (%) – Eq. 6	55.1	72.4	62.0
Error (%)	6.0	2.4	0.5

Permeability

Figure 6 shows the change of permeability with relative density. The samples became permeable at a relative density of 95% ($E_D = 32.4$ J/mm^3) and permeability increases linearly until a relative density of 80%. At relative densities below 80% ($E_D < 20$ J/mm^3), there is a sharp increase in permeability, which then increases linearly at almost the same rate as that above 80%. Permeability of verification samples (shown as ×) are also included in the figure and shows a similar relationship. The effect of energy density on permeability is shown in Fig. 7. Overall, the graph exhibits the same trend as in Fig. 6. However, at energy density below 20 J/mm^3, the rate of increase with decreasing energy density was higher. The sudden increase in permeability observed can be attributed to the volume of open pores which can be seen in Fig. 4. At energy densities below 20 J/mm^3, the incomplete formation of struts at each layer created a large volume of through pores from the top to the bottom surface, leading to the marked
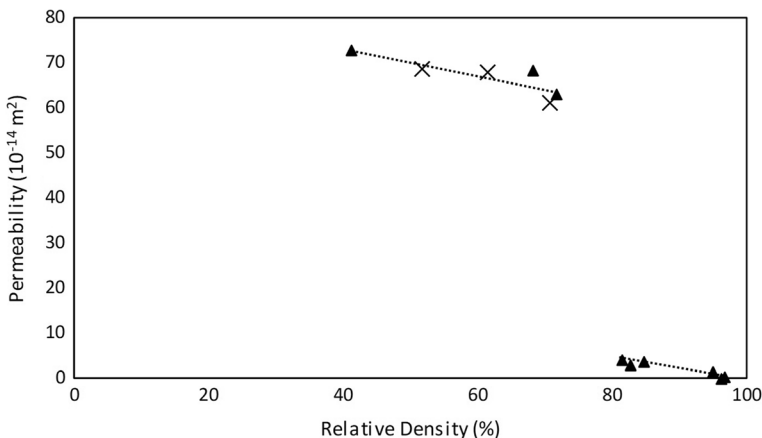
Fig. 6 Graph of permeability against relative density. × represents data of verification samples
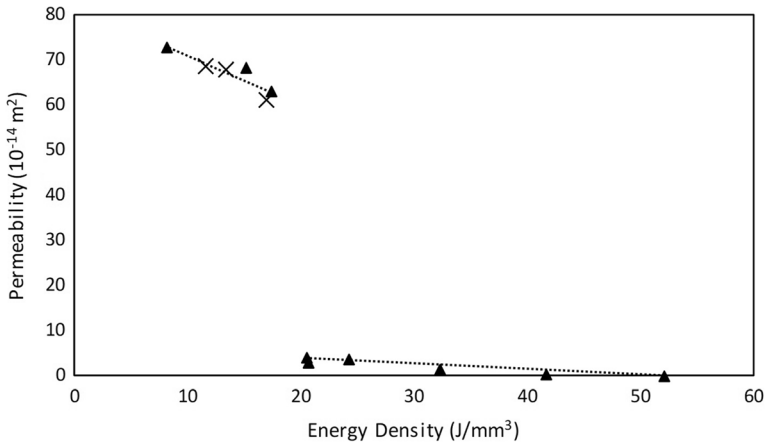
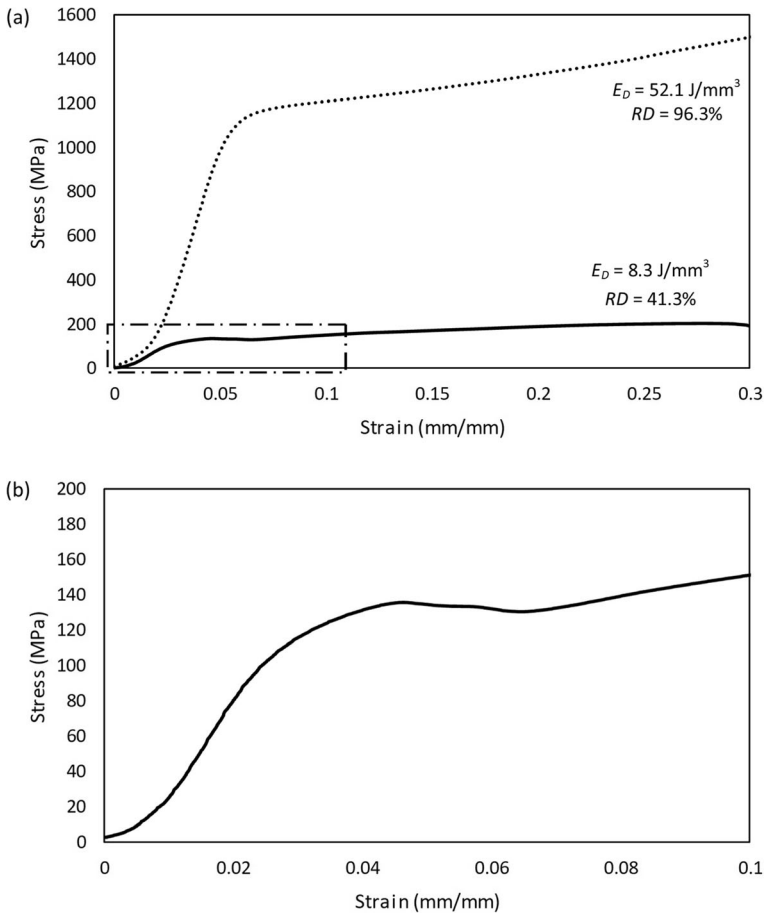**Fig. 7** Graph of permeability against energy density. × represents data of verification samples

Fig. 8 Stress-strain curve for (**a**) the highest and the lowest relative density specimen, and (**b**) enlarged portion of the stress-strain curve for the lowest density specimen
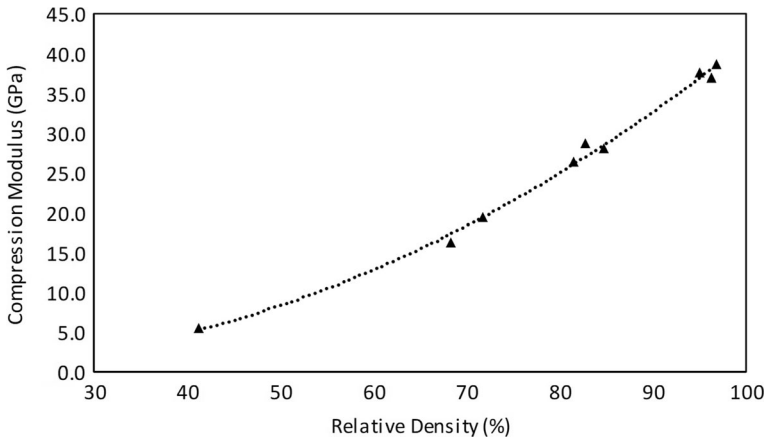
Fig. 9 Variation in compression elastic modulus against the relative density of the specimens

increase in permeability. At energy densities between 20 and 32 J/mm³, even though pores are present at layer, the complete formation of struts in each layer resulted in the reduction in the number of through pores and the size of the pores, reducing the permeability. At even higher energy densities, struts are completely formed, leaving only a few open pores between the struts, limiting the permeability of the samples.

Compression Properties

Representatives of the stress-strain curves from the compression tests are shown in Fig. 8. All specimens, except the lowest relative density specimens, show the same characteristic curve as in Fig. 8a for the specimen at a relative density of 96.3%. There is no clear yield point and the transition from elastic to plastic is continuous. For the lowest relative density specimen, there is a clear yield point, after which the stress decreases slightly before increasing again. This section is enlarged and shown in Fig. 8b.

Figures 9 and 10 show the graph of compression elastic modulus, E^*, and compression yield strength, $\sigma_{y,0.2}$, against relative density. When the relative density
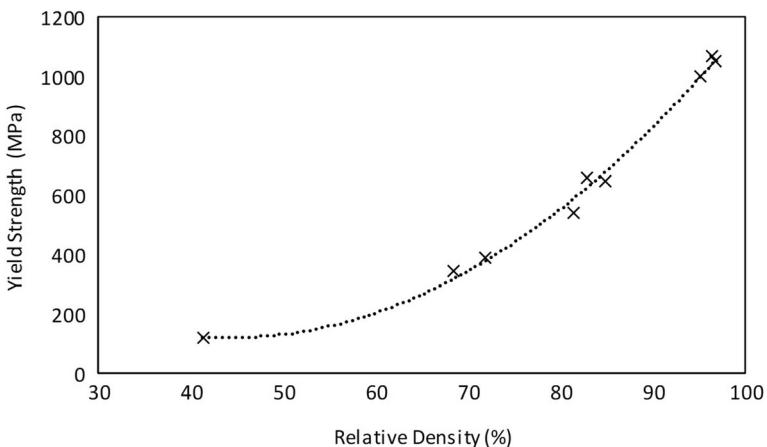

Fig. 10 Variation in compression yield strength against the relative density of the specimens

increases, both elastic modulus and yield strength also increases. This is expected as more materials are available to withstand the load. The modulus and yield strength of the specimens manufactured using the standard parameter values were found to be 38.3 $\pm$ 0.6 GPa and 1057 $\pm$ 12 MPa respectively. At the lowest relative density of 41%, the modulus and yield strength are 5.6 $\pm$ 0.2 GPa and 140 $\pm$ 5 MPa respectively, which are only 15% and 13% of the value, respectively. This is due to the pore structure seen in Fig. 4a where most of the struts are not connected.

Conclusions

Porous maraging 300 steel specimens were successfully fabricated by controlling the processing parameters of the SLM process with a relative density as low as 41%. Four processing parameters were investigated, namely laser power, scanning speed, layer thickness, and hatch spacing. From the DOE, hatch spacing was found to be the most important parameter, followed by laser power, layer thickness, and scanning speed. The four processing parameters can also be related by an energy density function which can be used to predict the relative density. The estimation of relative density using the energy density function is better than using the regression equation combining all four processing parameters. The samples became permeable at a relative density of 95% and permeability increases gradually down to a relative density of 80%. At relative densities below 80%, corresponding to energy densities below 20 J/mm^3, a sharp increase in permeability was observed, which is due to the increasing number of open pores present. As expected, the compression properties decrease with decreasing relative density. At the lowest relative density of 41%, both compression modulus and yield strength were only 15% and 13%, respectively, of the highest density sample. This research has shown that it is possible to build porous and non-porous section into the same part by changing the processing parameters at different sections of the part. This method can save time and cost for manufacturers as compared to using lattice structures. Porous metallic materials in this study are proven to have permeability properties that allow air particles to pass through, serving as a potential air vent in injection moulds. For future work, the heat transfer properties in porous metallic materials will be studied to further improve heat exchanging properties of the injection moulds to allow moulds to cool down faster.

Data Availability   Not applicable.

Compliance with Ethical Standards

Conflict of Interest   The authors declare that they have no known competing financial interests or personal relationships that could have appeared to influence the work reported in this paper.

Code Availability   Not applicable.

References

1. Kennedy, A.: Porous Metals and Metal Foams Made from Powders. In: Kondoh, K. (ed.) Powder Metallurgy, pp. 32–46. IntechOpen (2012). https://doi.org/10.5772/33060
2. Qin, J., Chen, Q., Yang, C., Huang, Y.: Research process on property and application of metal porous materials. J. Alloys Compd. **654**, 39–44 (2016). https://doi.org/10.1016/j.jallcom.2015.09.148
3. Yang, X., Yu, J., Guo, Z., Jin, L., He, Y.: Role of porous metal foam on the heat transfer enhancement for a thermal energy storage tube. Appl. Energy. **239**, 142–156 (2019). https://doi.org/10.1016/j.apenergy.2019.01.075
4. Qingbo, A., Jianzhong, W., Hao, Z.: Sound absorption characteristics and structure Optimiza- tion of porous metal fibrous Materials. Rare Metal Mater. Eng. **44**(11), 2646–2650 (2015). https://doi.org/10.1016/S1875-5372(16)60011-5
5. Davis, J.R. (ed.): Casting, Forming, and Forging. In: Gear Materials, Properties, and Manufacture. ASM International, Materials Park (2005)
6. Prakash, K.S., Nancharaih, T., Rao, V.V.S.: ScienceDirect additive manufacturing techniques in manufacturing - an overview. Mater. Today Proc. **5**(2), 3873–3882 (2018). https://doi.org/10.1016/j.matpr.2017.11.642
7. Malca, C., Santos, C., Sena, M., Mateus, A.: Development of SLM cellular structures for injection molds manufacturing. Sci. Technol. Mater. **30**(1), 13–22 (2018). https://doi.org/10.1016/j.stmat.2018.03.001
8. Xue, W., Krishna, B.V., Bandyopadhyay, A., Bose, S.: Processing and biocompatibility evaluation of laser processed porous titanium. Acta Biomater. **3**(6), 1007–1018 (2007). https://doi.org/10.1016/j.actbio.2007.05.009
9. Beyer, C., Figueroa, D.: Design and analysis of lattice structures for additive manufacturing. J. Manuf. Sci. Eng. **138**(12), 121014 (2016). https://doi.org/10.1115/1.4033957
10. Helou, M., Kara, S.: Design, analysis and manufacturing of lattice structures: an overview. Int. J. Comput. Integr. Manuf. **31**(3), 243–261 (2018). https://doi.org/10.1080/0951192X.2017.1407456
11. Hanzl, P., Zetek, M., Bakša, T., Kroupa, T.: The influence of processing parameters on the mechanical properties of SLM parts. Procedia Eng. **100**, 1405–1413 (2015). https://doi.org/10.1016/j.proeng.2015.01.510
12. Tucho, W.M., Lysne, V.H., Austbø, H., Sjolyst-Kverneland, A., Hansen, V.: Investigation of effects of process parameters on microstructure and hardness of SLM manufactured SS316L. J. Alloys Compd. **740**, 910–925 (2018). https://doi.org/10.1016/j.jallcom.2018.01.098
13. Gu, H., Gong, H., Pal, D., Rafi, K., Starr, T., Stucker, B.: Influences of Energy Density on Porosity and Microstructure of Selective Laser Melted 17- 4PH Stainless Steel. In: Proceedings of the Solid Freeform Fabrication Symposium, Austin, TX, pp. 474–489 (2013)
14. Liverani, E., Toschi, S., Ceschini, L., Fortunato, A.: Effect of selective laser melting (SLM) process parameters on microstructure and mechanical properties of 316L austenitic stainless steel. J. Mater. Process. Technol. **249**, 255–263 (2017). https://doi.org/10.1016/j.jmatprotec.2017.05.042
15. Kurzynowski, T., Gruber, K., Stopyra, W., Kuźnicka, B., Chlebus, E.: Correlation between process parameters, microstructure and properties of 316 L stainless steel processed by selective laser melting. Mater. Sci. Eng. A. **718**, 64–73 (2018). https://doi.org/10.1016/j.msea.2018.01.103
16. Khorasani, A., Gibson, I., Awan, U.S., Ghaderi, A.: The effect of SLM process parameters on density, hardness, tensile strength and surface quality of Ti-6Al-4V. Addit. Manuf. **25**, 176–186 (2019). https://doi.org/10.1016/j.addma.2018.09.002
17. Mugwagwa, Y.: Matope: effect of process parameters on residual stresses, distortions, and porosity in selective laser melting of Maraging steel 300. Metals (Basel). **9**(1042), (2019). https://doi.org/10.3390/met9101042
18. Tonelli, L., Fortunato, A., Ceschini, L.: CoCr alloy processed by selective laser melting (SLM): effect of laser energy density on microstructure, surface morphology, and hardness. J. Manuf. Process. **52**, 106–119 (2020). https://doi.org/10.1016/j.jmapro.2020.01.052
19. Stamp, R., Fox, P., O'Neill, W., Jones, E., Sutcliffe, C.: The development of a scanning strategy for the manufacture of porous biomaterials by selective laser melting. J. Mater. Sci. Mater. Med. **20**(9), 1839–1848 (2009). https://doi.org/10.1007/s10856-009-3763-8
20. Bandyopadhyay, A., Espana, F., Balla, V.K., Bose, S., Ohgami, Y., Davies, N.M.: Influence of porosity on mechanical properties and in vivo response of Ti6Al4V implants. Acta Biomater. **6**(4), 1640–1648 (2010). https://doi.org/10.1016/j.actbio.2009.11.011

21. Balla, V.K., Bodhak, S., Bose, S., Bandyopadhyay, A.: Porous tantalum structures for bone implants: fabrication, mechanical and in vitro biological properties. Acta Biomater. **6**(8), 3349–3359 (2010). https://doi.org/10.1016/j.actbio.2010.01.046

22. Ahsan, M.N., Paul, C.P., Kukreja, L.M., Pinkerton, A.J.: Porous structures fabrication by continuous and pulsed laser metal deposition for biomedical applications; modelling and experimental investigation. J. Mater. Process. Technol. **211**(4), 602–609 (2011). https://doi.org/10.1016/j.jmatprotec.2010.11.014

23. Zhang, S., Wei, Q., Cheng, L., Li, S., Shi, Y.: Effects of scan line spacing on pore characteristics and mechanical properties of porous Ti6Al4V implants fabricated by selective laser melting. Mater. Des. **63**, 185–193 (2014). https://doi.org/10.1016/j.matdes.2014.05.021

24. Furumoto, T., Koizumi, A., Alkahari, M.R., Anayama, R., Hosokawa, A., Tanaka, R., Ueda, T.: Permeability and strength of a porous metal structure fabricated by additive manufacturing. J. Mater. Process. Technol. **219**, 10–16 (2015). https://doi.org/10.1016/j.jmatprotec.2014.11.043

25. Ahmadi, S.M., Hedayati, R., Ashok Kumar Jain, R.K., Li, Y., Leeflang, S., Zadpoor, A.A.: Effects of laser processing parameters on the mechanical properties, topology, and microstructure of additively manufactured porous metallic biomaterials: A vector-based approach. Mater. Des. **134**, 234–243 (2017). https://doi.org/10.1016/j.matdes.2017.08.046

26. Seo, J.-Y., Shim, D.-S.: Effect of track spacing on porosity of metallic foam fabricated by laser melting deposition of Ti6Al4V/TiH 2 powder mixture. Vacuum. **154**, 200–207 (2018). https://doi.org/10.1016/j.vacuum.2018.04.058

27. Seo, J.Y., Lee, K.Y., Shim, D.S.: Effects of process parameters on properties of porous foams formed by laser-assisted melting of steel powder (AISI P21)/foaming agent (ZrH2) mixture. Opt. Laser Technol. **98**, 326–338 (2018). https://doi.org/10.1016/j.optlastec.2017.08.008

28. Enneti, R.K., Morgan, R., Atre, S.V.: Effect of process parameters on the selective laser melting (SLM) of tungsten. Int. J. Refract. Met. Hard Mater. **71**, 315–319 (2018). https://doi.org/10.1016/j.ijrmhm.2017.11.035

Publisher's Note Springer Nature remains neutral with regard to jurisdictional claims in published maps and institutional affiliations.

Affiliations

Shen Huei Wynton Lee[1] · **Hui Leng Choo**[1] · **Sui Him Mok**[2] · **Xin Yi Cheng**[3] · **Yupiter Harangan Prasada Manurung**[4]

[1] School of Computer Science and Engineering, Taylor's University, No. 1 Jalan Taylor's, 47500 Subang Jaya, Malaysia

[2] SLM Solutions Singapore Pte Ltd, 25 International Business Park, #02-15/17 German Centre, Singapore 609916, Singapore

[3] Omni Mold Ltd, 51 Joo Koon Circle, Singapore 629069, Singapore

[4] Faculty of Mechanical Engineering, UiTM Shah Alam, Shah Alam, Selangor, Malaysia